Hydrothermal Synthesis of Monodisperse Magnetite Nanoparticles

T. J. Daou,*,† G. Pourroy,† S. Bégin-Colin,*,† J. M. Grenèche,‡ C. Ulhaq-Bouillet,† P. Legaré,§ P. Bernhardt,§ C. Leuvrey,† and G. Rogez†

Institut de Physique et Chimie des Matériaux de Strasbourg, UMR CNRS-ULP 7504, 23 rue du Loess, BP 43, 67034 Strasbourg Cedex 2, France, Laboratoire de Physique de L'Etat Condensé, UMR CNRS 6087, Université du Maine, 72085 Le Mans Cedex 9, France, and Laboratoire des Matériaux, Surfaces et Procédés pour la Catalyse (LMSPC), UMR 7515, CNRS-ECPM, Université Louis Pasteur, 25 rue Becquerel, 67087 Strasbourg Cedex 2, France

Received April 6, 2006. Revised Manuscript Received June 19, 2006

Magnetite particles with an average size of 39 nm and good monodispersity have been synthesized by coprecipitation at 70 °C from ferrous Fe^{2+} and ferric Fe^{3+} ions by a $(N(CH_3)_4OH)$ solution, followed by hydrothermal treatment at 250 °C. The magnetite nanoparticles before the hydrothermal step display an average size of 12 nm and are highly oxidized when they are in contact with air. Complementary microstructural and magnetic characterizations of nanoparticles after hydrothermal treatment show unambiguously that they consist of magnetite with only a slight deviation from stoichiometry ($\delta \approx 0.05$), leading to $Fe_{2.95}O_4$.

1. Introduction

Among all iron oxides, magnetite Fe_3O_4 presents the most interesting properties because of the presence of iron cations in two valence states, Fe^{2+} and Fe^{3+}, in the inverse spinel structure. Magnetic properties of magnetite nanoparticles have been widely studied because of their relevance to magnetic recording, biomedical applications, etc.[1−5]

Moreover, the synthesis of magnetite nanoparticles with a controlled size has long been of scientific and technological interest. Indeed, the reduction of the particle size leads to new and original properties, particularly magnetic properties (superparamagnetism).[2,6] Various synthetic methods have been reported in the literature for the preparation of nanoscale Fe_3O_4 particles with grain sizes smaller than 20 nm, such as the reduction of hematite Fe_2O_3 by CO,[7,8] coprecipitation of an aqueous solution of ferrous and ferric ions by a base,[9−12] oxidation of the ferrous hydroxide gels using KNO_3,[13] γ-ray irradiation,[14] microwave plasma synthesis,[15] polyol-mediated sol−gel,[16] sonochemistry,[17] oil-in-water emulsion route using a small amount of cyclohexane as the oil phase,[18] microwave hydrothermal reaction,[19,20] nonaqueous route,[21−23] etc.

On the contrary, the process toward higher (20 nm < d < 100 nm) monodisperse magnetite nanoparticles has had only limited success, although such nanoparticles are of great interest, mainly for hyperthermia.[3−5] Indeed, one interest of magnetite nanoparticles with grain sizes larger than 20 nm is their ferrimagnetic behavior at room temperature. To the best of our knowledge, few detailed magnetic studies have been reported because of difficulties encountered with obtaining a monodisperse magnetite particle size larger than 20 nm and controlling the stoichiometry.

Moreover, controlling the synthesis conditions is a critical point, because the properties of nanoparticles are found to vary with synthesis methods.[19,20,24−29] The variations in

* Corresponding author. E-mail: daou@ipcms.u-strasbg.fr (T.J.D.); begin@ipcms.u-strasbg.fr (S.B.-C.). Fax: 33 3-88-10-72-47. Tel: 33 3-88-10-71-92.
† Institut de Physique et Chimie des Matériaux de Strasbourg.
‡ Université du Maine.
§ Université Louis Pasteur.

(1) Bate, G. In *Ferromagnetic Materials, Recording Materials*; Wohlfarth, E. D., Ed.; North-Holland: Amsterdam, 1980; Vol. 2, p 381.
(2) Raj, K.; Moskowitz, R. J. *J. Magn. Magn. Mater.* **1990**, *85*, 233.
(3) Mornet, S.; Vasseur, S.; Grasset, F.; Duguet, E. *J. Mater. Chem.* **2004**, *14*, 2161.
(4) Ito, A.; Shinkai, M.; Honda, H.; Kobayashi, T. *J. Biosci. Bioeng.* **2005**, *100* (1), 1.
(5) Shinkai, M. *J. Biosci. Bioeng.* **2002**, *94* (6), 606.
(6) Leslie-Pelecky, D. L.; Rieke, R. D. *Chem. Mater.* **1996**, *8*, 1770.
(7) Darken, L. S.; Gurry, P. W. *J. Am. Chem. Soc.* **1946**, *68*, 79.
(8) Osterhout, V. In *Magnetic Oxides*; Craik, D. S., Ed.; Wiley: New York, 1975; p 700.
(9) Shen, L.; Laibinis, P. E.; Hatton, T. A. *Langmuir* **1999**, *447*, 7.
(10) Sugimoto, T.; Matijevic, E. *J. Colloid Interface Sci.* **1980**, *74*, 1980.
(11) Kang, Y. S.; Risbud, S.; Rabolt, J. F.; Stroeve, P. *Chem. Mater.* **1996**, *8*, 2209.
(12) Fried, T.; Shemer, G.; Markovich, G. *Adv. Mater.* **2001**, *13*, 1158.
(13) Visalakshi, G.; Venkataswaran, G.; Kulshreshtha, S. K.; Moorthy, P. N. *Mater. Res. Bull.* **1993**, *28*, 829.
(14) Wang, S.; Xin, H.; Qian, Y. *Mater. Lett.* **1997**, *33*, 113.
(15) Vollath, D.; Szabo, D. V. *J. Mater. Res.* **1997**, *12*, 2175.
(16) Feldmann, C.; Jungk, H.-O. *Angew. Chem., Int. Ed.* **2001**, *40*, 359.
(17) Vijaya Kumar, R.; Koltypin, Y.; Cohen, Y.; Aurbach, D.; Palchik, O.; Felner, I.; Gedanken, A. *J. Mater. Chem.* **2000**, *10*, 1125.
(18) Zhou, Z. H.; Wang, J.; Liu, X.; Chan, H. S. O. *J. Mater. Chem.* **2001**, *11*, 1704.
(19) Khollam, Y. B.; Dhage, S. R.; Potdar, H. S.; Deshpande, S. B.; Bakare, P. P.; Kulkarni, S. D.; Date S. K. *Mater. Lett.* **2001**, *56*, 571.
(20) Dhage, S. R.; Khollam, Y. B.; Potadr, H. S.; Beshpande, S. B.; Bakare, P. P.; Sainkar, S. R.; Date, S. K. *Mater. Lett.* **2002**, *57*, 457.
(21) Sun, S.; Zeng, H. J. *J. Am. Chem. Soc.* **2002**, *124*, 8204.
(22) Pinna, N.; Grancharov, S.; Beato, P.; Bonville, P.; Antonietti-Niederberger, M. *Chem. Mater.* **2005**, *17*, 3044.
(23) Li, Z.; Chen, H.; Bao, H.; Gao, M. *Chem. Mater.* **2004**, *16*, 1391.
(24) Goya, G. F.; Berquo, T. S.; Fonseca, F. C. *J. Appl. Phys.* **2003**, *94*, 3520.
(25) Shebanova, O. N.; Lazor, P. J. *J. Solid State Chem.* **2003**, *174*, 424.
(26) Belin, T.; Guigue-Millot, N.; Caillot, T.; Aymes, D.; Niepce, J. C. *J. Solid State Chem.* **2002**, *163*, 459.
(27) Voogt, F. C.; Palstra, T. T. M.; Nielsen, L.; Rogojanu, O. C.; James, M. A.; Hibma, T. *Phys. Rev. B* **1998**, *57*, R8107.
(28) Voogt, F. C.; Fuji, T.; Smulders, P. J. M., Nielsen, L.; James, M. A.; Hibma, T. *Phys. Rev. B* **1999**, *60*, 11193.

10.1021/cm060805r CCC: $33.50
Published on Web 08/04/2006

magnetic properties were assigned to different parameters, such as cationic distribution and vacancies, nonstoichiometry, spin canting, or surface contribution due to the nanometric size.[23,24,30−35] Reports on the synthesis of magnetite nanoparticles with controlled grain sizes and careful characterizations have been unable to choose between these explanations.

We report here the synthesis of magnetite nanoparticles, with an average grain size of 39 ± 5 nm, a controlled stoichiometry, and a ferrimagnetic behavior at room temperature, by using a hydrothermal process. A hydrothermal process is one of the successful ways of growing crystals of many different materials such as quartz, malachite, etc. This technique has also been used to grow dislocation-free single-crystal particles, and grains formed in this process could have a better crystallinity than those from other processes. The nanoparticles before and after hydrothermal treatment are characterized carefully, and results are discussed on the basis of magnetization curve, ZFC/FC (zero-field cooling/field cooling) and Mössbauer measurements.

2. Experimental Details

2.1. Materials. The chemical reagents used in this work were ferrous chloride tetrahydrate ($FeCl_2 \cdot 4H_2O$), ferric chloride hexahydrate ($FeCl_3 \cdot 6H_2O$), tetramethylammonium hydroxide ($(N(CH_3)_4OH)$, 25%), and hydrochloric acid. All the chemical reagents were of analytical grade.

2.2. Synthesis of Magnetite Nanoparticles. Distilled water, degassed with argon gas for half an hour, was used for the preparation of 1 M $FeCl_3 \cdot 6H_2O$ and 2 M $FeCl_2 \cdot 4H_2O$ by dissolving iron salts in 2 M HCl solutions.

In a typical experimental procedure, 10 mL of a 1 M $FeCl_3$ solution was mixed with 2.5 mL of a 2 M $FeCl_2$ solution in a flask. The mixture was heated to 70 °C under argon while being stirred with a mechanical stirrer, followed by the slow addition of 21 mL of a 25% aqueous solution of $N(CH_3)_4OH$.

Vigorous stirring was carried on for 20 min. The solution color could be seen changing from orange to black, leading to a black precipitate, and the mixture was then dropped into the Teflon-lined stainless autoclave. During the experiment, argon was continuously passed through the solution to prevent the oxidation of the Fe^{2+} in the system. The autoclave was then put in an oven at 250 °C for 24 h and slowly cooled to room temperature naturally.

The product was isolated by applying a permanent magnet. The supernatant was discarded by decantation. Degassed water was then added to wash the precipitates. This procedure was repeated three to four times to remove excess ions and tetramethylammmonium salt in the suspension, and finally the precipitated powder was dried using a freeze dryer.

Maghemite γ-Fe_2O_3 was obtained by heating magnetite at 300 °C for 12h.

2.4. Characterization of Particles. X-ray diffraction (XRD) data were collected at room temperature using a D500 Siemens diffractometer equipped with a quartz monochromator (Co $K\alpha_1$ = 0.17890 nm). The lattice parameter calculations were obtained using UFIT software.[36] The average crystallite size was estimated using the Debye−Scherrer equation, $\Delta(2\theta) = 0.9\lambda/(L\cos(\theta_0))$. X-ray photoelectron spectroscopy (XPS) was performed using a ThermoVGScientific photoelectron spectrometer equipped with a twin anode, providing both unchromatized Al Kα and Mg Kα radiations (1486.6 and 1453.6 eV, respectively). The spectrometer, which was equipped with a multichannel detector, operated in the constant resolution mode with a pass energy of 20 eV. The total resolution of the system was estimated to be 0.55 eV.

The specific surface areas were determined by BET-N_2 adsorption. The particle sizes were deduced using the relation ϕ (nm) = $6000/\mu S$, where ϕ is the particle diameter, μ the density, and S the specific surface. TG and DT analysis were performed using a TA Instruments apparatus with a heating rate of 5 °C/min in air. The morphology of the particles was observed by scanning electron microscopy (SEM) using a JEOL electron microscope 6700 coupled with EDX spectroscopy. TEM and HRTEM images were recorded with a TOPCON model 002B transmission electron microscope, operating at 200 kV, with a point-to-point resolution of 0.18 nm. Raman-scattering experiments were carried out using a micro-Raman system at room temperature. The 514.53 nm line of an Ar^+ laser with an exposure time of 300 s was used for excitation. ^{57}Fe Mössbauer spectra were performed at 300 and 77 K using a conventional constant acceleration transmission spectrometer with a $^{57}Co(Rh)$ source and a bath cryostat. The spectra were fitted by means of the MOSFIT program,[37] and an α-Fe foil was used as the calibration sample.

ZFC/FC measurements were performed using a superconducting quantum interference device (SQUID) magnetometer (Quantum Design model MPMS-XL) between 4 and 400 K. Hysteresis cycles were recorded at room temperature by using a vibrating sample magnetometer.

3. Results and Discussion

3.1. Structural Characterization. The X-ray diffraction patterns recorded on the powders before (BT) and after (HT) the hydrothermal treatment are presented in Figure 1. All detected diffraction peaks can be indexed in the spinel structure, indicating that the sample contains neither crystalline hematite (α-Fe_2O_3) nor iron hydroxides. Moreover, the (210) and (211) X-ray peaks of maghemite (Figure 1c) are not observed in the XRD patterns of nanoparticles before and after hydrothermal treatment (panels a and b of Figure 1). The calculated lattice parameters *a* are 0.8379 ± 0.0004 nm and 0.8393 ± 0.0002 nm before and after the hydrothermal step, respectively, and have to be compared to the maghemite (γ-Fe_2O_3) and magnetite (Fe_3O_4) ones, 0.8346 nm (JCPDS file 39-1346) and 0.8396 nm (JCPDS file 19-629), respectively. Before hydrothermal treatment, the phase

(29) Guigue-Millot, N.; Champion, Y.; Hÿtch, M. J.; Bernard, F.; Begin-Colin, S.; Perriat, P. *J. Phys. Chem. B* **2001**, *105*, 7125.
(30) Paramês, M. L.; Mariano, J.; Rogalski, M. S.; Popovici, N.; Conde, O. *Mater. Sci. Eng., B* **2005**, *118*, 246.
(31) Dormann, J. L.; Fiorani, D.; Tronc, E. *Adv. Chem. Phys.* **1997**, *98*, 282.
(32) Tronc, E.; Fiorani, D.; Noguès, M.; Testa, A. M.; Lucari, F.; D'Orazio, F.; Grenèche, J. M.; Wernsdorfer, W.; Galvez, N.; Chanéac, C.; Mailly, D.; Verdaguer, M.; Jolivet, J.-P. *J. Magn. Magn. Mater.* **2003**, *262*, 6.
(33) Tronc, E.; Ezzir, A.; Cherkaoui, R.; Chanéac, C.; Noguès, M.; Kachkachi, H.; Fiorani, D.; Testa, A. M.; Grenèche, J. M.; Jolivet, J.-P. *J. Magn. Magn. Mater.* **2000**, *221*, 63.
(34) Chinnasamy, C. N.; Narayanasamy, A.; Ponpandian, N.; Chattopadhyay, K.; Guérault, H.; Greneche, J. M. *J. Phys.: Condens. Matter* **2000**, *12*, 7795.
(35) Ponpandian, N.; Narayanasamy, A.; Chinnasamy, C. N.; Sivakumar, N.; Greneche, J. M.; Chattopadhyay, K.; Shinoda, K.; Jeyadevan, B.; Tohji, K. *Appl. Phys. Lett.* **2005**, *86*, 192510.
(36) Evain, M. Unpublished UFIT program; Institut des Materiaux de Nantes: Nantes, France.
(37) Teillet, J.; Varret, F. Unpublished MOSFIT program; Université du Maine; le Mans, France.

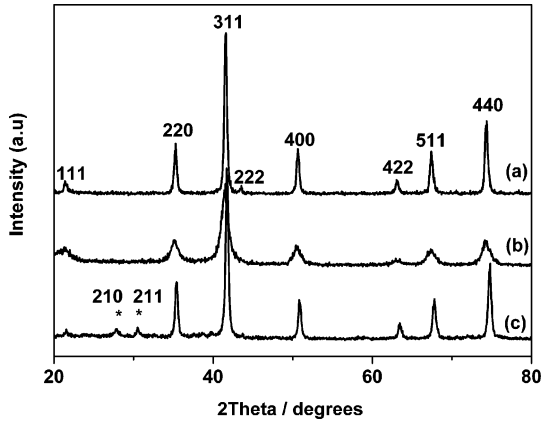

Figure 1. XRD patterns of the Fe_3O_4 nanoparticles (a) after and (b) before hydrothermal treatment and of (c) maghemite. The positions of the additional peaks of the maghemite structure are marked with asterisks (*).

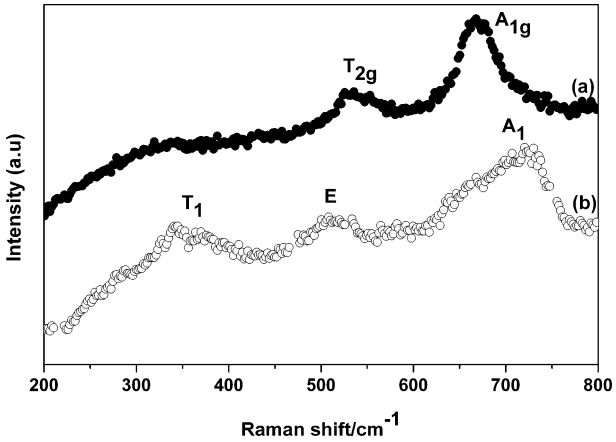

Figure 2. Raman spectra of (a) synthesized samples of Fe_3O_4 after hydrothermal treatment and (b) γ-Fe_2O_3.

Table 1. Lattice Parameter and Crystallite Size of Magnetite before and after Hydrothermal Treatment from XRD Results and Average Grain Sizes Deduced from BET Measurements and TEM Observations

T (°C)	lattice parameter (nm)	Φ_{XRD}(nm)	S (m^2/g)	Φ_{BET} (nm)	Φ_{TEM} (nm)
70	0.8379 ± 0.004	12 ± 2	117	10 ± 2	12 ± 2
250 (HT)	0.8393 ± 0.002	39 ± 5	31	38 ± 5	40 ± 5

has an intermediate lattice parameter, showing that a partial oxidation probably occurs in air. Indeed, Fe^{2+} cations in nanoparticles are not thermodynamically stable under air.[26,29,38] Because of their nanometric sizes, they are easily oxidized into Fe^{3+}. The cell parameter decreases quite linearly as the deviation from stoichiometry (δ in $Fe_{3-3\delta}O_4$)[26,39] increases; by taking into account the value of the cell parameter of magnetite before hydrothermal treatment, we expect a large oxidation of about 65% of the Fe^{2+} cations.[26] Moreover, a relationship between the stoichiometric deviation δ in magnetite $Fe_{3-\delta}O_4$ and the lattice parameter reported by Yang et al. gives $\delta \approx 0.09-0.1$.[40] After hydrothermal treatment, the crystalline phase has a lattice parameter very close to the magnetite one. Indeed, the same relationship gives, in our case, $Fe_{2.96\pm0.01}O_4$. This deviation in stoichiometry may be attributed, as for nanoparticles before hydrothermal treatment, to a surface oxidation of Fe^{2+}, showing that the hydrothermal step leads to an improved stoichiometry of powders.

Raman spectroscopy also allows us to differentiate the iron oxide phases.[22,25,40−42] The Raman spectrum of HT nanoparticles is displayed in Figure 2, together with the maghemite one. It exhibits the characteristic bands of magnetite at 668 and 535 cm^{-1} assigned to the A_{1g} and T_{2g} transitions, which can be easily distinguished from maghemite ones at 720, 500, and 350 cm^{-1}.[22,25,40−42]

The average crystallite sizes of the powder before and after the hydrothermal treatment have been estimated using several methods (Table 1). First, the Debye−Scherrer formula used from the (311) reflection leads to 12 ± 2 nm for BT nanoparticles and 39 ± 5 nm for HT nanoparticles. These values are in agreement with those calculated from the BET surface area measurements (Table 1). SEM and TEM micrographs confirm the homogeneous particle size distribution of HT magnetite nanoparticles (Figure 3 and Figure 4a). Indeed, the average particle size (from the counting of about 100 particles) of magnetite nanoparticles before and after hydrothermal treatment is 12 ± 2 nm and 40 ± 5 nm. The electron diffraction pattern measured from a large zone (Figure 4b) presents spots/rings that can be indexed to the magnetite structure. The HRTEM image shown in Figure 4c exhibits planes with interplanar distances of 0.48 nm that are characteristic of (111) spinel planes. No stacking faults are visible. The growth axis is [111] as often observed for magnetite particles. These observations and the good agreement between the average particle sizes determined by several methods suggest that the nanoparticles are monocrystalline and quite monodisperse.

TG and DT analyses in air for HT magnetite and maghemite appear in Figure 5. The TGA curve of HT magnetite displays a weight loss from room temperature

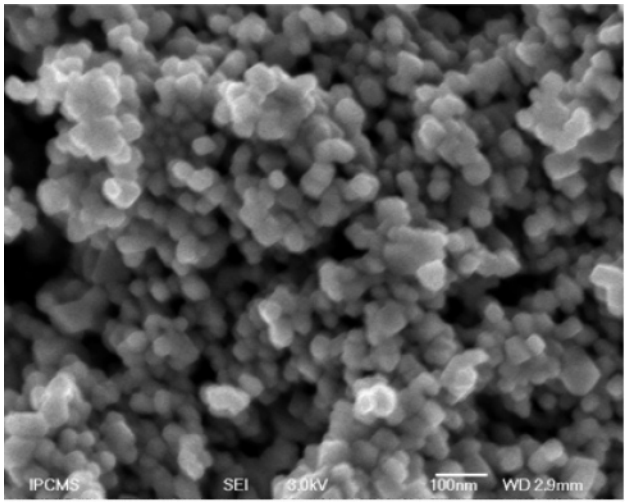

Figure 3. Scanning electron microscopy (SEM) image of Fe_3O_4 after hydrothermal treatment.

(38) Jolivet, J.-P.; Tronc, E. *J. Colloid Interface Sci.* **1998**, *125*, 688.
(39) Poix, P. *Liaisons interatomiques et propriétés physiques des composes minéraux*; Suchet: Paris, 1996.
(40) Yang, J. B.; Zhou, X. D.; Yelon, W. B.; James, W. J.; Cai, Q.; Gopalakrishnan, K. V.; Malik, S. K.; Sun, X. C.; Nikles, D. E. *J. Appl. Phys.* **2004**, *95*, 7540.
(41) Cornell, R. M.; Schwertmann, U. *The Iron Oxides*; VCH: New York, 1996; p 135.
(42) De Faria, D. L. A.; Venancio Silva, S.; De Oliveira, M. T. *J. Raman Spectrosc.* **1997**, *28*, 873.

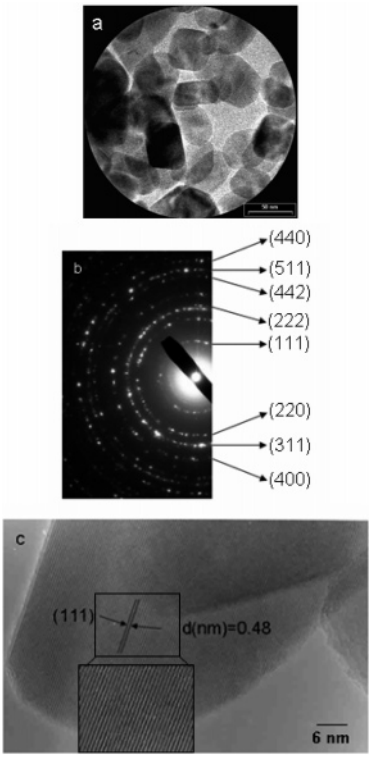

Figure 4. (a) TEM micrograph, (b) selected area electron diffraction (SAED) pattern acquired from a 39 nm Fe_3O_4 nanoparticle assembly, and (c) HRTEM of magnetite nanoparticle after hydrothermal treatment.

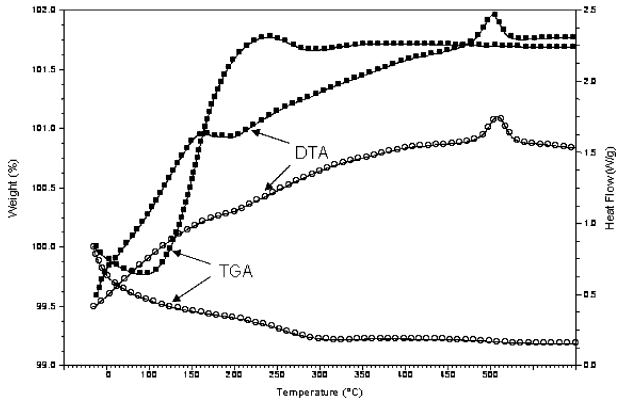

Figure 5. DTA/TGA curves of HT magnetite (solid circle) and maghemite (open circle) nanoparticles.

followed by a weight gain between 100 and 200 °C and a weak loss above 250 °C. This complex behavior results from the simultaneous dehydration of the powder and oxidation of Fe^{2+}. The transformation of magnetite into maghemite corresponds to the feature at around 160 °C in the DTA curve.[41] This is confirmed by the DTA/TGA experiment conducted on maghemite: no feature is observed on any curves except the weight loss due to dehydration of powders. The competition between dehydration and oxidation of Fe^{2+} prevents us from evaluating the weight gain corresponding to Fe^{2+} oxidation in HT magnetite. The final phase transformation of maghemite into hematite is observed at around 500 °C.[43] This was also confirmed by the DTA/TGA experiment conducted on maghemite, where a similar feature is observed at around 500 °C in the DTA curve.

(43) Xisheng, Y.; Dongsheng, L.; Zhengkuan, J.; Lide, Z. *J. Phys. D: Appl. Phys.* **1998**, *31*, 2734.

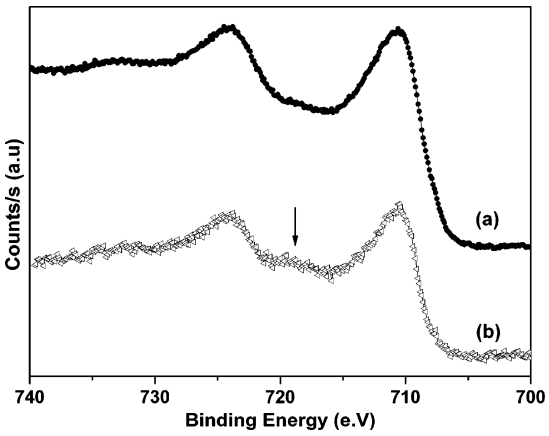

Figure 6. Fe 2p peaks in the XPS spectra of Fe_3O_4 nanoparticles (a) after and (b) before hydrothermal treatment.

XPS spectra given in Figure 6 display bands assigned to Fe (2p) in magnetite before and after hydrothermal treatment. The Fe^{3+} and Fe^{2+} ions are distinguishable by XPS. Indeed, when Fe^{2+} ions are present at the surface, the satellite of the 2p3/2 peak around 719 eV characteristic of the Fe^{3+} ions in γ-Fe_2O_3 becomes less resolved, mainly because of the main 2p3/2 and 2p1/2 peaks broadening and the rising intensity of the Fe^{2+} satellite at about 716 eV. Moreover, a peak shoulder is observed around 709 eV, the intensity of which decreases when the stoichiometric deviation in $Fe_{3-\delta}O_4$ increases.[44−47] The presence of Fe^{2+} at the surface of the hydrothermal magnetite is confirmed by the quasiabsence of the satellite around 719 eV between the main Fe 2p peaks (arrow in Figure 6) and the presence of a faint shoulder below 710 eV. By contrast, this satellite is observed in the XPS spectrum of magnetite before hydrothermal treatment together with a reduction of the contribution around 709 eV. Nevertheless, the intensity of the shoulder at 709 eV is quite low in the HT magnetite spectrum, confirming that some surface oxidation of Fe^{2+} has occurred. However, the comparison of these spectra shows that Fe^{2+} ions are always observed on the surface of HT magnetite nanoparticles and supports the idea that the HT magnetite nanoparticles do not present a layer of maghemite at their surface.

3.2. Mössbauer Spectrometry. Main characterization techniques show that the powders consist of magnetite. However, more-specialized techniques such as Mössbauer spectrometry are useful for determining the oxidation degree and the distribution of cations, whereas magnetic measurements are needed for describing the magnetic behavior of the synthesized magnetite phase. As shown in Figure 7, the Mössbauer spectra at both 300 and 77 K seem similar to those usually observed for magnetite. At 300 K, one distinguishes two resolved sextets, one attributed to Fe^{3+} in the A site of spinel magnetite (the outer sextet) and one attributed to $Fe^{2.5+}$ in the B site; the Mössbauer spectrum at 77 K displays a sextet with broadened and symmetrical lines, as expected. The latter spectrum can be well-described using

(44) Aronniemi, J. P.; Sainio, J.; Lahtinen, J. *Surf. Sci.* **2005**, *578*, 108.
(45) Jung Chu, W. *Magn. Reson. Imaging* **1995**, *13*, 675.
(46) Fujii, T.; de Groot, F. M. F.; Sawatzky, G. A.; Voogt, F. C.; Hibma, T.; Okada, K. *Phys. Rev. B* **1999**, *59*, 3195.
(47) Kendelewicz, T.; Liu, P.; Doyle, C. S.; Brown, G. E., Jr.; Nelson, E. J.; Chambers S. A. *Surf. Sci.* **2000**, *453*, 32.

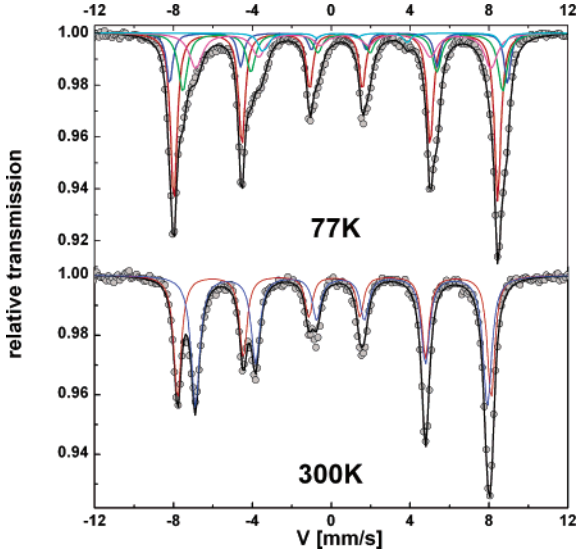

Figure 7. Mössbauer spectra of HT magnetite nanoparticles at 300 and 77 K.

Table 2. ^{57}Fe Mössbauer Parameters for HT Magnetite Recorded at 300 and 77K

	isomer shift relative to α-Fe[a] (mm/s)	width at half -height[a] (mm/s)	quadrupole shift[a] (mm/s)	hyperfine field[b] (T)	relative subspectral area[c] (%)
		300 K			
A	0.32	0.46	−0.00	49.1	45
B	0.66	0.53	0.04	45.7	55
		77 K			
	0.40	0.40	0.00	50.7	42
	0.54	0.41	−0.04	52.8	14
	0.78	0.61	−0.03	49.9	25
	0.86	0.69	0.02	46.0	15
	1.15	0.70	2.19	34.5	4

[a] Standard deviation equal to ±0.01. [b] Standard deviation equal to ±0.2. [c] Standard deviation equal to ±1.

at least five components that are attributed to Fe^{3+} located in tetrahedral sites, Fe^{3+} in octahedral sites, Fe with intermediate valence states, and Fe^{2+} in octahedral sites. The values of the hyperfine parameters, which are listed in Table 2, are consistent with those generally reported for magnetite, except for the sextet area leading to a $Fe^{3+}_{tetra}/Fe^{3+,2+}_{octa}$ ratio of 0.81, whereas the theoretical ratio is equal to 0.50, and for the content of Fe^{2+} at 77 K, which is known to be about 10%.[19,48] It is important to emphasize that the intensity ratio of sextet A to sextet B is very sensitive to the stoichiometry of magnetite.[13,19,40,49,50] The intensity ratio, which exceeds 0.50, is generally attributed to a superstoichiometry in oxygen or cationic vacancies. In the present study, there would be oxidation of Fe^{2+} on the B site in Fe^{3+} accompanied by vacancy formation, giving the general formula $Fe^{3+}_A[Fe^{2.5+}_{2-6\delta}Fe^{3+}_{5\delta\leq\delta}]_BO_4^{2-}$. Calculations of the stoichiometry deviation from relative subspectral area with two different reported formulas, $\delta = 0.063$ in $Fe_{3-\delta}O_4$[28] and $\delta = 0.057$ in $Fe_{3-\delta}O_4$,[30] give a general formula of $Fe_{2.94}O_4$. The values of the isomer shift lead to an estimate of the Fe valence state, i.e., the Fe content; assuming the isomer shift of Fe^{3+}_{tetra}, Fe^{3+}_{octa}, and Fe^{2+}_{octa} at 0.25, 0.40, and 1.00 at 300 K, and 0.40, 0.54, and 1.15 at 77 K, respectively, one obtains $Fe_{2.95}O_4$. Thus, the HT nanoparticles consist of magnetite with a slight deviation from stoichiometry, leading to an $Fe_{2.95}O_4$ compound. Comparison of the spectra at 77 K with those obtained with γ-Fe_2O_3−Fe_3O_4 solid solutions with similar stoichiometry deviations[51] shows that the hydrothermally synthesized magnetite is not such a solid solution. Indeed, if the Mössbauer spectra are similar at 300 K, they are different at 77 K, as the spectrum is deconvoluted with only two sextets for the solid solution. It confirms XPS results, i.e., that the stoichiometry deviation is due to the presence of oxidized Fe^{2+} ions at the surface of the nanoparticle.

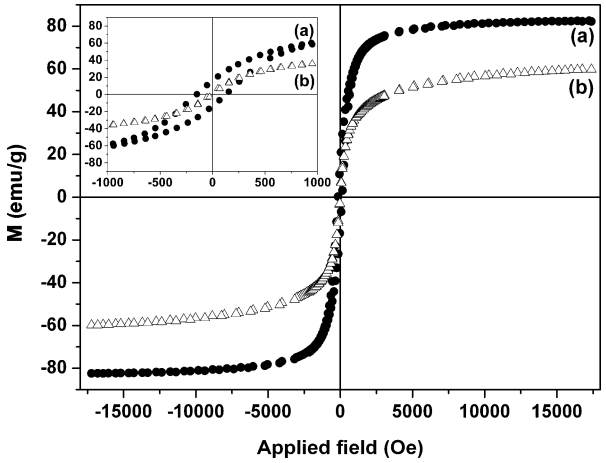

Figure 8. Magnetization curve at room temperature of magnetite nanoparticles (a) after and (b) before hydrothermal treatment.

Nevertheless, the value of the isomer shift of Fe^{3+} in the A site is higher than that generally reported for the micrometric magnetite. This suggests that some charge transfers might occur also in the A site, which could be due to a cationic distribution not as ideal as in bulk magnetite.

3.3. Magnetic Measurements.

Figure 8 shows a typical magnetization curve and hysteresis loop for the nanoparticles. The saturation magnetizations of the particles before and after hydrothermal treatment are 59.8 and 82.5 emu/g, respectively. Those values are lower than the theoretical value of the bulk magnetite (92 emu/g),[52] as already observed by Goya et al. (75.6 emu/g for 150 nm nanoparticles)[24] and Panda et al. (67.8 emu/g for 12 nm nanoparticles).[53] A decrease in M_s is often observed with nanoparticles and is attributed to the surface contribution: spin canting, surface disorder, stoichiometry deviation, cation distribution, and adsorbed species (water) as evidence from TGA experiments.[24,53] The temperature dependence of the ZFC and FC magnetization for HT magnetite is presented in Figure 9. The ZFC curve displays two transition temperatures: one around 122 K that corresponds to the Verwey transition temperature (T_V) of pure magnetite and the other at about 50 K, previously reported and attributed to a spin-

(48) Doriguetto, A. C.; Fernandes, N. G.; Persiano, A. I. C.; Nunes Filho, E.; Grenèche, J. M.; Fabris, J. D. *Phys. Chem. Miner.* **2003**, *30*, 249.
(49) Balasubramaniam, C.; Khollam, Y. B.; Banerjee, I.; Bakare, P. P.; Date, S. K.; Das, A. K.; Bhoraskar, S. V. *Mater. Lett.* **2004**, *58*, 3958.
(50) Simmons, G. W.; Leidheiser, H., Jr. *Application of Mössbauer Spectroscopy*; Cohen, R. L., Ed.; Academic Press: New York, 1976; Vol. 1, p 106.
(51) Schmidbauer, E.; Keller, M. *J. Magn. Magn. Mater*. **2006**, *297*, 107.
(52) Han, D. H.; Wang, H. L.; Luo, J. *J. Magn. Magn. Mater*. **1994**, *136*, 176.
(53) Panda, R. N.; Gajbhiye, N. S.; Balaji, G. *J. Alloys Compd*. **2001**, *326*, 50.

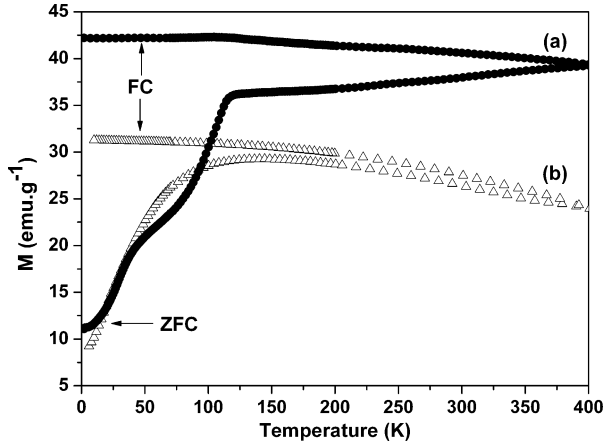

Figure 9. ZFC/FC curves of magnetite nanoparticles (a) after and (b) before hydrothermal treatment under a field of 500 Oe.

glass transition or spin reorientation of Fe magnetic moments.[40] Further characterizations, such as frequency-dependent ac susceptibility measurements, will be performed to clear up this phenomena. The value of T_V is similar to that reported for bulk magnetite.[54] T_V has been reported to be very sensitive to the stoichiometry, because the Fe vacancy increase in the $Fe_{3-\delta}O_4$ leads to a decrease in the strength of the Fe−Fe exchange on B sites. Indeed, T_V is reported to decrease from $Fe_{2.995}O_4$ at 125 K to $Fe_{2.934}O_4$ at 100 K. This is clearly observed in magnetite nanoparticles obtained before hydrothermal treatment, which present large deviations from stoichiometry (Figure 9); T_V is identified at around 100 K, and no transition is observed at 50 K. Thus, the HT magnetite nanoparticles, which display a stoichiometry deviation, should present a decrease in T_V. The position of T_V at 122 K and the Mössbauer results, which show that the powders are not a γ-Fe_2O_3−Fe_3O_4 solid solution, confirm that only the surface of nanoparticles presents a stoichiometry deviation and that the main volume is made of stoichiometric magnetite. These results, high oxidation of Fe^{2+} in 12 nm nanoparticles, and only surface oxidation in 39 nm nanoparticles are in agreement with the fact that Fe^{2+} oxidation increases with decreasing particle size. The nonstoichiometric part certainly explains the observed decrease in saturation magnetization by comparison with the bulk values.

(54) Aragon, R.; Shepherd, J. P.; Koenitzer, J. W.; Buttrey, D. J.; Rasmussen, R. J.; Honig, J. M. *J. Appl. Phys.* **1985**, *57*, 3221.

4. Conclusion

We have successfully prepared magnetite nanoparticles with an average size of 39 nm and a good monodispersity by a hydrothermal process using a ($N(CH_3)_4OH$) solution as a base. XRD and TEM studies reveal that the hydrothermal process leads to the formation of larger grains with controlled stoichiometry. The different techniques of characterization lead to a complete and unambiguous characterization of HT magnetite powders and let us say that the nanoparticles consist of magnetite slightly oxidized on the surface with a global composition of $Fe_{2.95}O_4$. The magnetic measurements show that the powder obtained after hydrothermal treatment has ferrimagnetic behavior at room temperature with saturation magnetization of 82.5 emu/g, near that of bulk magnetite. The microstructural and magnetic characterizations of the two types of synthesized magnetite nanoparticles lead us to claim that the stoichiometry of magnetite has an important effect on the magnetic properties.

CM060805R